SGN – Assignment #2

Marcello Mutti, 220252

Disclaimer: The story plot contained in the following three exercises is entirely fictional.

Exercise 1: Uncertainty propagation

The Prototype Research Instruments and Space Mission Technology Advancement (PRISMA) is a technology in-orbit test-bed mission for demonstrating Formation Flying (FF) and rendezvous technologies, as well as flight testing of new sensors and actuator equipment. It was launched on June 15, 2010, and it involves two satellites: Mango (Satellite 1, ID 36599), the chaser, and Tango (Satellite 2, ID 36827), the target.

You have been provided with an estimate of the states of Satellites 1 and 2 at the separation epoch t_{sep} = `2010-08-12T05:27:39.114` (UTC) in terms of mean and covariance, as reported in Table 1. Assume Keplerian motion can be used to model the spacecraft dynamics.

1. Propagate the initial mean and covariance for both satellites within a time grid going from t_{sep} to $t_{sep} + N\,T_1$, with a step equal to T_1, where T_1 is the orbital period of satellite 1 and $N = 10$, using both a Linearized Approach (LinCov) and the Unscented Transform (UT). We suggest to use $\alpha = 0.1$ and $\beta = 2$ for tuning the UT in this case.

2. Considering that the two satellites are in close formation, you have to guarantee a sufficient accuracy about the knowledge of their state over time to monitor potential risky situations. For this reason, at each revolution, you shall compute:

   - the norm of the relative position (Δr), and
   - the sum of the two covariances associated to the position elements of the states of the two satellites (P_{sum})

   The critical conditions which triggers a collision warning is defined by the following relationship:

   $$\Delta r < 3\sqrt{\max(\lambda_i(P_{\text{sum}}))}$$

   where $\lambda_i(P_{\text{sum}})$ are the eigenvalues of P_{sum}. Identify the revolution N_c at which this condition occurs and elaborate on the results and the differences between the two approaches (UT and LinCov).

3. Perform the same uncertainty propagation process on the same time grid using a Monte Carlo (MC) simulation *. Compute the sample mean and sample covariance and compare them with the estimates obtained at Point 1). Provide the plots of:

   - the time evolution for all three approaches (MC, LinCov, and UT) of $3\sqrt{\max(\lambda_i(P_{r,\text{i}}))}$ and $3\sqrt{\max(\lambda_i(P_{v,\text{i}}))}$, where $i = 1, 2$ is the satellite number and P_r and P_v are the 3x3 position and velocity covariance submatrices.
   - the propagated samples of the MC simulation, together with the mean and covariance obtained with all methods, projected on the orbital plane.

   Compare the results and discuss on the validity of the linear and Guassian assumption for uncertainty propagation.

*Use at least 100 samples drawn from the initial covariance

Table 1: Estimate of Satellite 1 and Satellite 2 states at t_0 provided in ECI J2000.

Parameter	Value
Ref. epoch t_{sep} [UTC]	2010-08-12T05:27:39.114
Mean state $\hat{\boldsymbol{x}}_{0,\text{sat1}}$ [km, km/s]	$\hat{\boldsymbol{r}}_{0,\text{sat1}} = [4622.232026629, 5399.3369588058, -0.0212138165769957]$ $\hat{\boldsymbol{v}}_{0,\text{sat1}} = [0.812221125483763, -0.721512914578826, 7.42665302729053]$
Mean state $\hat{\boldsymbol{x}}_{0,\text{sat2}}$ [km, km/s]	$\hat{\boldsymbol{r}}_{0,\text{sat2}} = [4621.69343340281, 5399.26386352847, -3.09039248714313]$ $\hat{\boldsymbol{v}}_{0,\text{sat2}} = [0.813960847513811, -0.719449862738607, 7.42706066911294]$
Covariance P_0 [km^2, km^2/s, km^2/s^2]	$\begin{bmatrix} +5.6e-7 & +3.5e-7 & -7.1e-8 & 0 & 0 & 0 \\ +3.5e-7 & +9.7e-7 & +7.6e-8 & 0 & 0 & 0 \\ -7.1e-8 & +7.6e-8 & +8.1e-8 & 0 & 0 & 0 \\ 0 & 0 & 0 & +2.8e-11 & 0 & 0 \\ 0 & 0 & 0 & 0 & +2.7e-11 & 0 \\ 0 & 0 & 0 & 0 & 0 & +9.6e-12 \end{bmatrix}$

1) Given the initial mean state of Mango, it is possible to compute the semi-major axis of the associated orbit exploiting the principle of conservation of energy:

$$\frac{\hat{\mathbf{v}}_{0,M}^2}{2} - \frac{\mu}{\hat{\mathbf{r}}_{0,M}} = -\frac{\mu}{2a_M}$$

Henceforth the subscripts $i = 1, 2$ will indicate $sat1$ and $sat2$ respectively, interchangeably with M and T.

The orbital period of Mango is therefore computed as:

$$T_1 = 2\pi\sqrt{\frac{a_M^3}{\mu}} = 6004.2399\,s = 1\,h\,40\,min\,4.2399\,s$$

In the case of the Linearized Approach method (LC), the mean propagated state $\hat{\mathbf{x}}^{LC}(t)$ can be simply computed as the propagated mean initial state.
Therefore, employing simple Keplerian Dynamics:

$$\begin{cases} \dot{\hat{\mathbf{r}}} = \hat{\mathbf{v}} & \hat{\mathbf{r}}(t_{sep}) = \hat{\mathbf{r}}_{0,i} \\ \dot{\hat{\mathbf{v}}} = -\mu\dfrac{\hat{\mathbf{r}}}{\hat{r}^3} & \hat{\mathbf{v}}(t_{sep}) = \hat{\mathbf{v}}_{0,i} \end{cases}$$

The subscript i refers to the satellite.

The function `KEPSTM` allows for the computation of both system dynamics and state transition matrix $\boldsymbol{\Phi}(t_{sep}, t)$ right hand side computation, so that both state and STM are propagated alongside:

$$\dot{\boldsymbol{\Phi}}(t_{sep}, t) = A(t)\,\boldsymbol{\Phi}(t_{sep}, t) \quad \boldsymbol{\Phi}(t_{sep}, t_{sep}) = I_{6\times6}$$
$$A(t) = \begin{bmatrix} 0 & I_{3\times3} \\ J & 0 \end{bmatrix} \qquad J = \frac{3\mu}{\hat{r}^5}\hat{\mathbf{r}}\hat{\mathbf{r}}^\intercal - \frac{\mu}{\hat{r}^3}I_{3\times3}$$

The integration is performed using MatLab's `ode113`, with absolute tolerance $AbsTol = 10^{-12}$ and relative tolerance $RelTol = 10^{-12}$. The same integrator and tolerances are employed throughout the rest of the assignment.

The state transition matrix is employed to propagate the satellites covariances:

$$P_i^{LC}(t) = \mathbf{\Phi}_i(t_{sep}, t)\, P(t_{sep})\, \mathbf{\Phi}_i^{\intercal}(t_{sep}, t) \quad P_i^{LC}(t_{sep}) = P_0$$

In the case of the Unscented Transform method (UT), the propagated mean state and covariance are computed as the weighted mean and covariance of the propagated σ-points. Starting from the UT tuning parameters $\alpha = 0.1$, $\beta = 2$, $k = 0$, given $n = 6$ the number of state elements, the mean $W_j^{(m)}$ and covariance $W_j^{(c)}$ weights are computed as follows:

$$\lambda = \alpha^2 (n + k) - n = -5.94$$

$$W_0^{(m)} = \frac{\lambda}{n+\lambda} = -99 \qquad W_j^{(m)} = \frac{1}{2(n+\lambda)} = 8.\overline{3} \quad \text{with} \quad j = 1:2n$$

$$W_0^{(c)} = W_0^{(m)} + (1 - \alpha^2 + \beta) \approx -96.01 \qquad W_j^{(c)} = \frac{1}{2(n+\lambda)} = 8.\overline{3} \quad \text{with} \quad j = 1:2n$$

The σ-points are propagated according to Keplerian dynamics from initial conditions computed at t_{sep} given $\hat{\mathbf{x}}_{0,i}$:

$$\mathbf{X}_{i,0}(t_{sep}) = \hat{\mathbf{x}}_{0,i}$$

$$\mathbf{X}_{i,j}(t_{sep}) = \hat{\mathbf{x}}_{0,i} + \left(\sqrt{(n+\lambda) P_0}\right)_j \qquad j = 1:n$$

$$\mathbf{X}_{i,j}(t_{sep}) = \hat{\mathbf{x}}_{0,i} - \left(\sqrt{(n+\lambda) P_0}\right)_{j-n} \qquad j = n+1:2n$$

Where $\left(\sqrt{(n+\lambda) P_0}\right)_j$ identifies the j^{th} column of $\sqrt{(n+\lambda) P_0}$.
At each time instant $t = t_{sep} + nT_1$, $n = 0:N$ the mean state and covariance:

$$\hat{\mathbf{x}}_i^{UT}(t) = \textstyle\sum_0^{j=2n} W_j^{(m)} \mathbf{X}_{i,j}(t)$$

$$P_i^{UT}(t) = \textstyle\sum_0^{j=2n} W_j^{(c)} \left[\mathbf{X}_{i,j}(t) - \hat{\mathbf{x}}_i^{UT}(t)\right] \left[\mathbf{X}_{i,j}(t) - \hat{\mathbf{x}}_i^{UT}(t)\right]^{\intercal}$$

Both satellites are characterized by low eccentricity orbits, approximately circular. Therefore, in particular in the case of Mango, the propagated mean state at each instant t is approximately constant.
Firstly, the result is therefore reported in terms of displacement of the LC computed mean $\hat{\mathbf{x}}_i^{LC}(t)$ with respect to initial mean state $\hat{\mathbf{x}}_{0,i}$:

$$\hat{\mathbf{x}}_1^{LC}(t) - \hat{\mathbf{x}}_{0,1}$$

n	r_x	r_y	r_z	v_x	v_y	v_z
1	-7.2760e-12	7.0031e-11	-3.8076e-10	2.3503e-13	2.8322e-13	-3.1974e-14
2	1.8190e-12	5.4570e-11	-2.7419e-10	1.5821e-13	1.9984e-13	-3.1974e-14
3	-2.8194e-11	8.1855e-11	-5.1545e-10	3.0931e-13	3.7914e-13	-2.9310e-14
4	2.6102e-10	8.3401e-10	-2.2233e-09	1.4611e-12	1.8996e-12	-8.6242e-13
5	5.8117e-10	1.2342e-09	-2.7633e-09	1.8336e-12	2.4303e-12	-1.3616e-12
6	9.5042e-10	1.6053e-09	-2.5273e-09	1.5010e-12	2.1337e-12	-1.8421e-12
7	1.2296e-09	1.4270e-09	-1.6606e-10	-9.9920e-15	3.9846e-13	-1.9513e-12
8	1.4898e-09	1.3033e-09	1.7647e-09	-1.2963e-12	-1.0766e-12	-2.0366e-12
9	1.7017e-09	1.1369e-09	3.5958e-09	-2.5487e-12	-2.5380e-12	-2.0526e-12
10	1.9490e-09	9.8953e-10	5.5304e-09	-3.9049e-12	-4.1059e-12	-2.1148e-12

$\hat{\mathbf{x}}_2^{LC}(t) - \hat{\mathbf{x}}_{0,2}$

n	r_x	r_y	r_z	v_x	v_y	v_z
1	6.3258e-02	-5.5945e-02	5.7734e-01	-3.9890e-04	-4.6601e-04	2.4182e-07
2	1.2648e-01	-1.1193e-01	1.1547e+00	-7.9781e-04	-9.3201e-04	4.3380e-07
3	1.8968e-01	-1.6794e-01	1.7320e+00	-1.1967e-03	-1.3980e-03	5.7596e-07
4	2.5285e-01	-2.2400e-01	2.3094e+00	-1.5956e-03	-1.8640e-03	6.6828e-07
5	3.1598e-01	-2.8009e-01	2.8867e+00	-1.9946e-03	-2.3300e-03	7.1078e-07
6	3.7908e-01	-3.3621e-01	3.4641e+00	-2.3935e-03	-2.7960e-03	7.0344e-07
7	4.4215e-01	-3.9237e-01	4.0414e+00	-2.7924e-03	-3.2620e-03	6.4628e-07
8	5.0519e-01	-4.4857e-01	4.6187e+00	-3.1914e-03	-3.7279e-03	5.3928e-07
9	5.6820e-01	-5.0481e-01	5.1961e+00	-3.5903e-03	-4.1939e-03	3.8245e-07
10	6.3118e-01	-5.6108e-01	5.7734e+00	-3.9893e-03	-4.6599e-03	1.7579e-07

There is a noticeable difference in orders of magnitude between $\hat{\mathbf{x}}_1^{LC}(t) - \hat{\mathbf{x}}_{0,1}$ and $\hat{\mathbf{x}}_2^{LC}(t) - \hat{\mathbf{x}}_{0,2}$. It is due to the fact that the time grid is defined upon Mango's orbital period T_1. Tango's orbit is characterized by a slightly lower period $T_2 = 6004.1621\,s$, therefore the apparent deviation with respect to $\hat{\mathbf{x}}_{0,2}$.

The results obtained via UT method are very close to those obtained with LC. The two methods are compared in terms of propagated mean position $\hat{\mathbf{r}}_i$ and propagated mean velocity $\hat{\mathbf{v}}_i$:

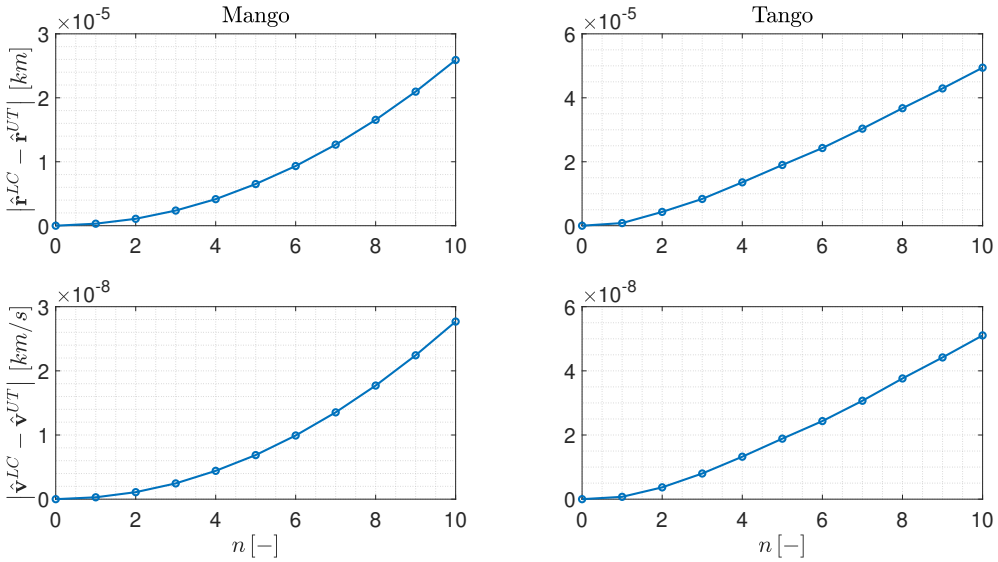

Figure 1: Propagated mean position $\hat{\mathbf{r}}$ and velocity $\hat{\mathbf{v}}$ method discrepancies.

The propagated covariances are presented in terms of $3\sqrt{tr\left(P(t)\right)}$. To better visualize the difference between the two methods, their discrepancies are also presented in terms of:

$$\left| 3\sqrt{tr\left(P(t)_i^{LC}\right)} - 3\sqrt{tr\left(P(t)_i^{UT}\right)} \right|$$

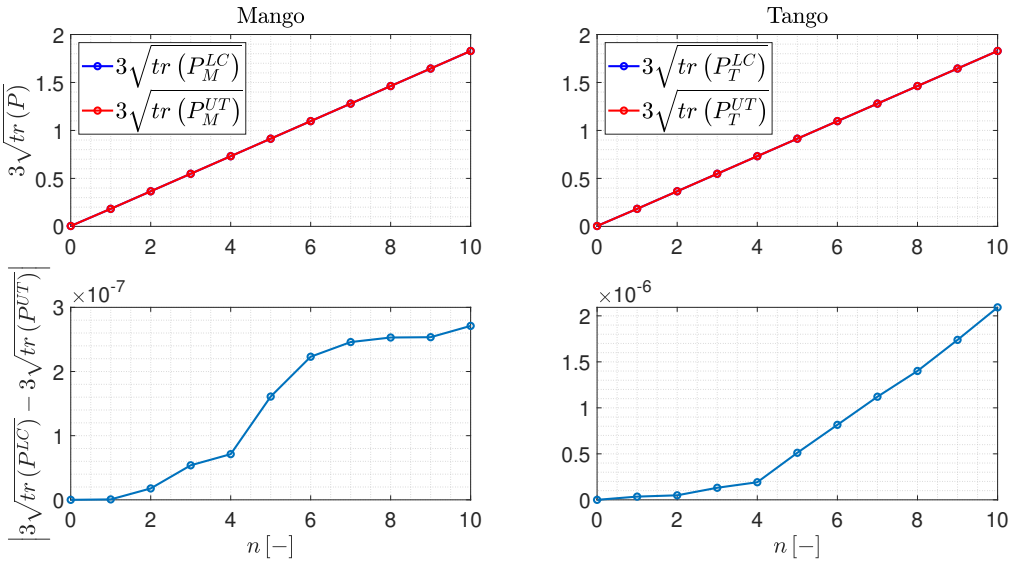

Figure 2: Propagated covariances and methods discrepancies.

2) The norm of the relative position is computed at each revolution as the norm of the difference of the mean states of the two satellites:

$$\Delta r\left(t\right) = \|\hat{\mathbf{x}}_T\left(t\right) - \hat{\mathbf{x}}_M\left(t\right)\|$$

The sum of the propagated covariances:

$$P_{sum}\left(t\right) = P_T\left(t\right) + P_M\left(t\right)$$

Below, the critical n_c collision warning for both the LC and UT method, computed as n associated to the first time instant over the defined time grid when the following inequality constraint is not satisfied:

$$\Delta r < 3\sqrt{max\left(\lambda_i\left(P_{sum}\right)\right)}$$

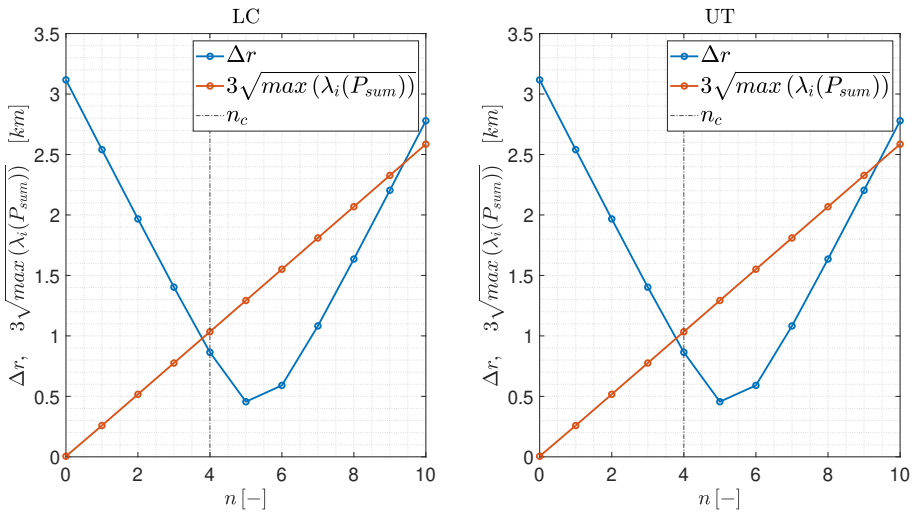

Figure 3: Critical condition n_c evaluation.

It is possible to observe that $n_c = 4$ regardless of the method employed.

In general, over the specified time grid the difference between the two methods is almost negligible in terms of both mean (Fig. 1) and covariance.

In particular it is highlighted the difference between the traces of P_{sum}^{UT} and P_{sum}^{LC}, in terms of $3\sqrt{max\left(\lambda_i\left(P_{sum}\right)\right)}$:

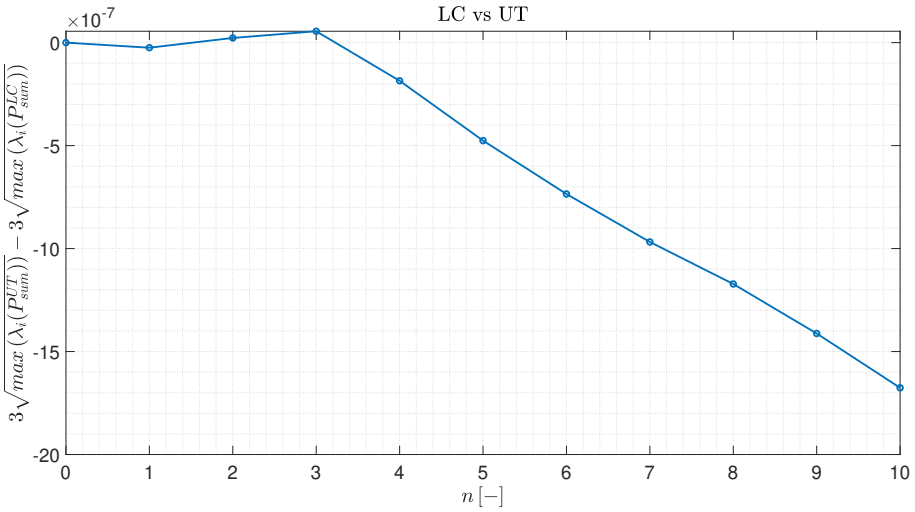

Figure 4: P_{sum} method comparison.

3) For the purpose of the computation of the Monte Carlo simulation, a population of $N_{MC} = 250$ samples is randomly generated for both Mango and Tango, given the respective mean initial state $\hat{\mathbf{x}}_{0,i}$ and common covariance P_0. The samples are propagated according to Keplerian dynamics over the previously defined time grid. At each time instant $t = t_{sep} + nT_1$, $n = 0 : N$ the sample mean state and covariance:

$$\hat{\mathbf{x}}_i^{MC}(t) = \frac{1}{N_{MC}} \sum_0^{k=N_{MC}} \mathbf{x}_{i,k}^{MC}(t)$$
$$P_i^{MC}(t) = \frac{1}{N_{MC}-1} \sum_0^{k=N_{MC}} \left[\mathbf{x}_{i,k}^{MC}(t) - \hat{\mathbf{x}}_i^{MC}(t)\right] \left[\mathbf{x}_{i,k}^{MC}(t) - \hat{\mathbf{x}}_i^{MC}(t)\right]^{\intercal}$$

It ought to be noted that given the random nature of the Monte Carlo process, each simulation yields a slightly different result. Increasing by number of samples N_{MC} helps stabilize the solution of the simulation.

Below the comparison over time of the maximum eigenvalue of both position and velocity covariance submatrices.
The maximum displacement with respect to MC associated with the plots reported below is 3.04%, computed for $3\sqrt{max\left(\lambda_i(P_{r,T})\right)}$.

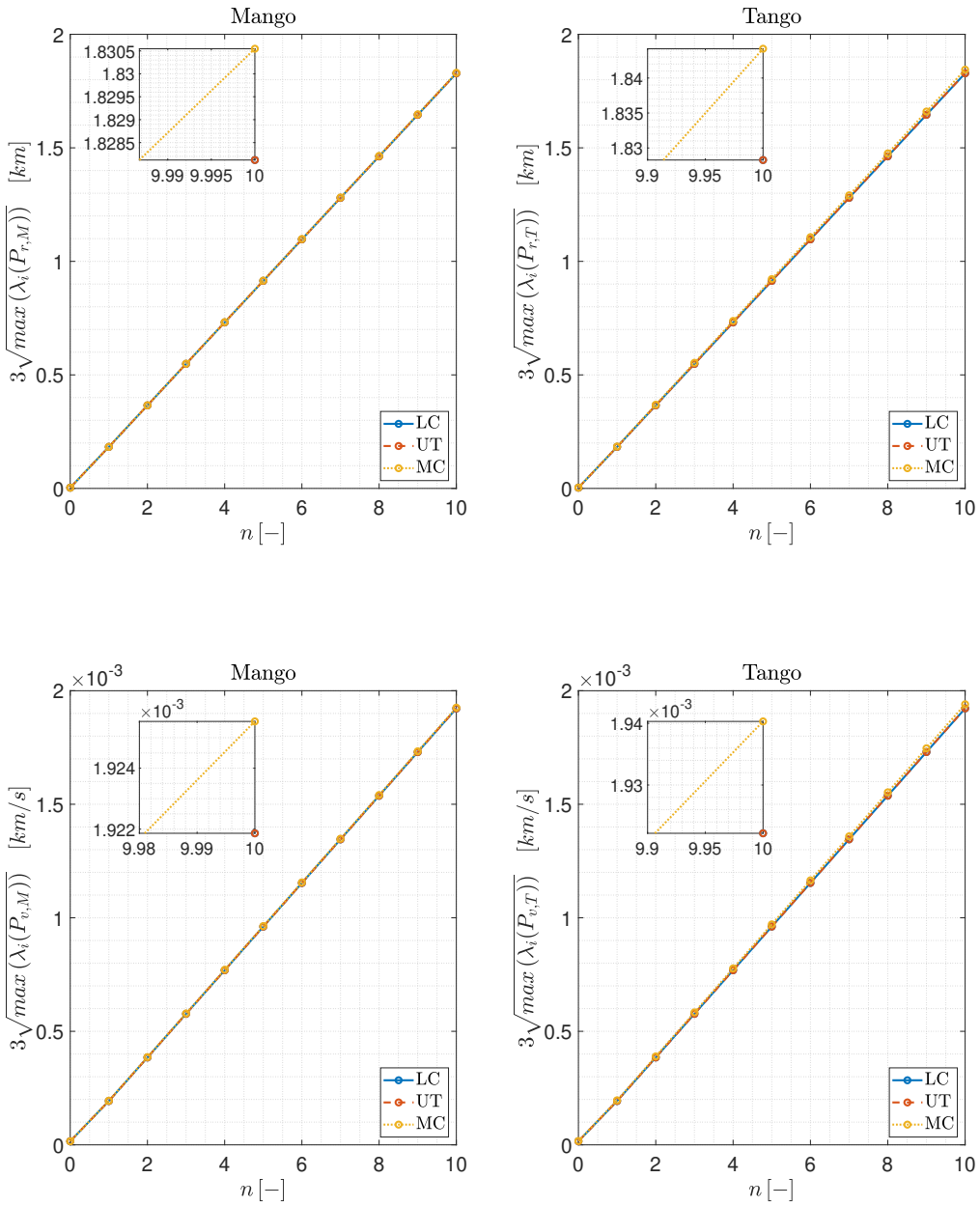

It is possible to visualize mean, covariance and propagated MC samples onto the orbital plane. It was chosen to represent those associated to $n = [1, 4, 7, 10]$.
Each of them is presented in the respective LVLH frame, in particular in the radial-transversal plane centered at $\hat{\mathbf{r}}_i^{LC}(t)$.

Given the rotation matrix $R_{LVLH/ECI}$, the covariance:

$$P_{LVLH,i}(t) = R_{LVLH/ECI,i}(t)\, P_{ECI,i}(t)\, R^{\intercal}_{LVLH/ECI,i}(t)$$

Given its 2×2 north-west minor $\widetilde{P}_{LVLH}$, its eigenvalues λ_i and eigenvectors $\mathbf{v}_i$, the 3σ gaussian covariance ellipse coordinates are computed as follows:

$$\begin{cases} x = 3\sqrt{\lambda_1}cos(\theta)sin(\phi) - 3\sqrt{\lambda_2}sin(\theta)sin(\phi) & \theta = atan\left(\dfrac{v_{1,y}}{v_{1,x}}\right) \\ y = 3\sqrt{\lambda_1}sin(\theta)cos(\phi) + 3\sqrt{\lambda_2}cos(\theta)sin(\phi) & \phi = 0 : 2\pi \end{cases}$$

Below the associated plots:

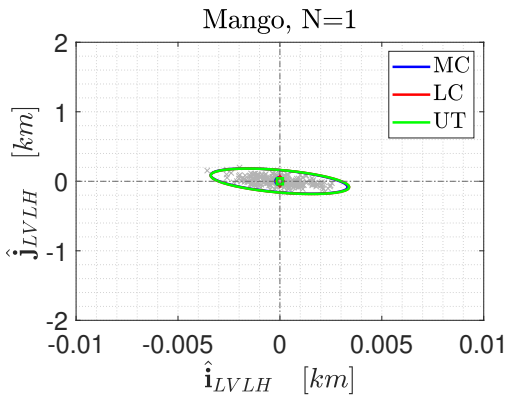

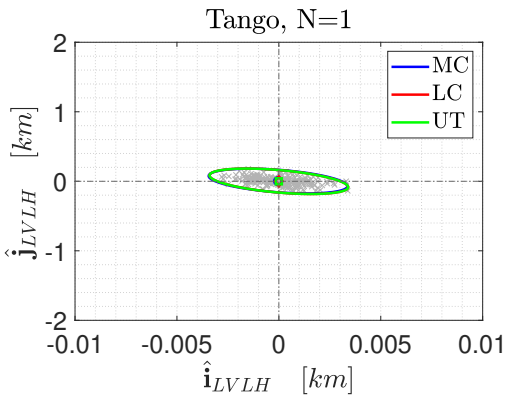

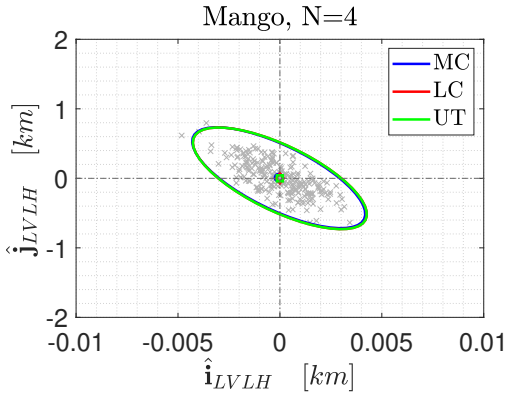

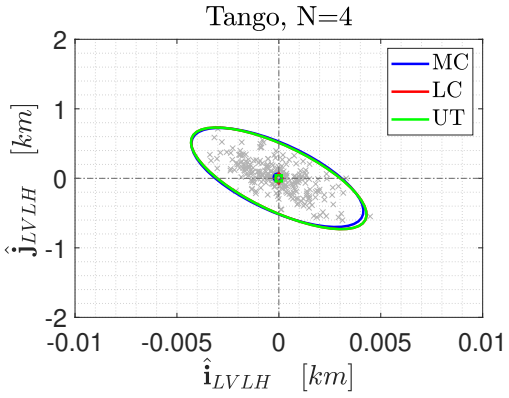

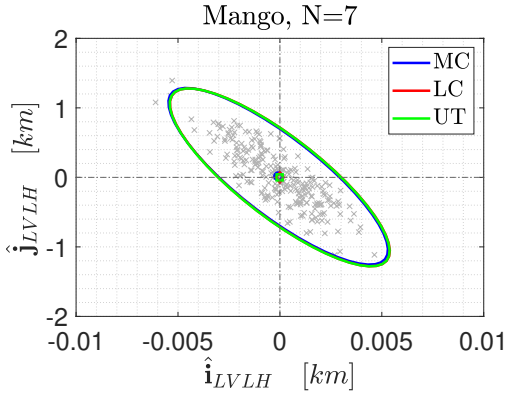

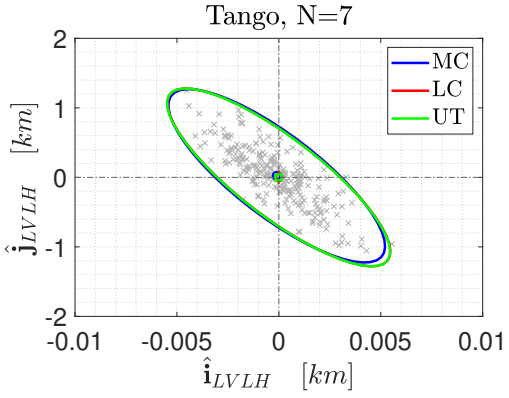

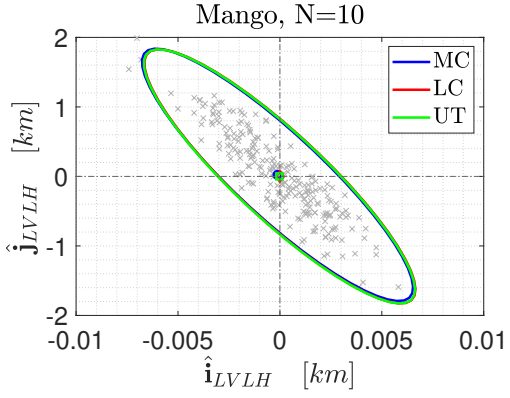

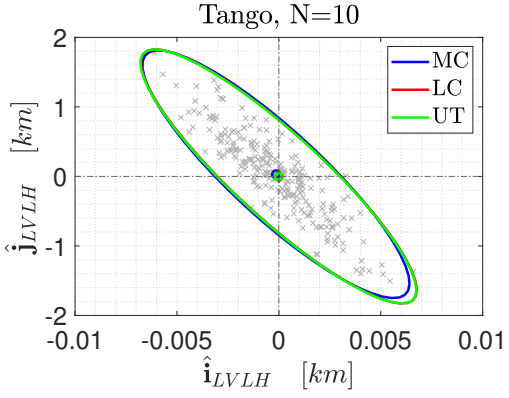

As expected, the covariances show the tendencies of growing in size and rotating towards the transversal direction $\hat{\mathbf{j}}_{LVLH}$.
The former behaviour is simply the reflection of the increase of uncertainty in function of propagation time.
The latter instead is explained by physical means. In fact, samples further away from the main body in the radial $\hat{\mathbf{i}}_{LVLH}$ direction are be characterized by higher orbital period, and therefore trail $\hat{\mathbf{r}}_i^{LC}$ at each revolution. On the other hand samples closer to the main body have higher angular velocity and therefore anticipate $\hat{\mathbf{r}}_i^{LC}$.
It ought to be noted that though the scales of the axes are consistent, they are very different: with equal axes the ellipses would appear qualitatively aligned with the transversal direction after just one revolution $n \geq 1$.

Both LC and UT methods share the hypothesis that the initial estimates in terms of both state and covariance are gaussian.
In the case of the UT, this hypothesis is only necessary for the starting conditions: mean and covariance are provided through sampling, with no regard for the propagated probability distribution. This allows UT to provide a reliable estimate even when the propagated samples are not gaussian.
On the other hand, since LC propagates the initial conditions through linearized dynamics, the propagated samples are expected to maintain the initial probability distribution. This is verified in the presence of linear or close to linear dynamics and for short propagation times.

In the study case, given $n \leq 10$, LC is capable of performing equally well with respect to UT. This is attributable to the nature of the propagated orbits, together with the dynamics employed: given the very low eccentricities the radii are approximately constant, therefore $\ddot{\hat{\mathbf{r}}}$ linearly proportional to $\hat{\mathbf{r}}$:

$$\begin{cases} k = \dfrac{\mu}{\hat{r}^3} \approx const \\ \ddot{\hat{\mathbf{r}}} = k\hat{\mathbf{r}} \end{cases}$$

Given that the covariance ellipses are in fact contour lines of multivariate gaussian probability density functions, the ability of LC to capture all but few outliers of the propagated MC samples validates the method assumptions.

However, even in the simplified case of circular orbits, such assumptions fall in the case of long propagation periods.
For example, at $n = 75$, the MC samples can be observed to form the so called Banana Shape Distribution:

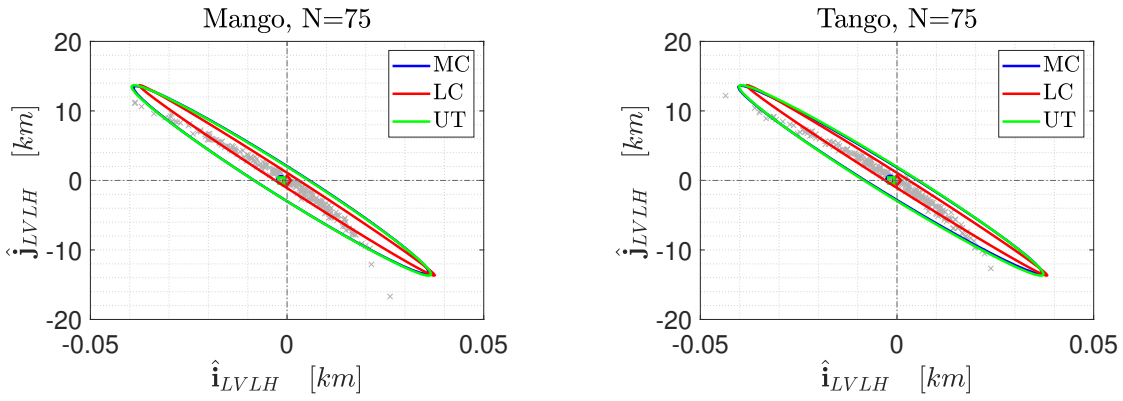

LC is therefore incapable of providing a reliable estimate. As previously stated, UT on the other hand provides a result much more descriptive of the real system behaviour, depicted by MC.

Exercise 2: Batch filters

You have been asked to track Mango to improve the accuracy of its state estimate. To this aim, you shall schedule the observations from the two ground stations reported in Table 4.

1. *Compute visibility windows.* By using the mean state reported in Table 1 and by assuming Keplerian motion, predict the trajectory of the satellite over a uniform time grid (with a time step of 60 seconds) and compute all the visibility time windows from the available stations in the time interval from t_0 = `2010-08-12T05:30:00.000` (UTC) to t_f = `2010-08-12T11:00:00.000` (UTC). Plot the resulting predicted Azimuth and Elevation profiles in the visibility windows.

2. *Simulate measurements.* The Two-Line Elements (TLE) set of Mango are reported in Table 2 (and in WeBeep as 36599.3le). Use SGP4 and the provided TLEs to simulate the measurements acquired by the sensor network in Table 4 by:

   (a) Computing the spacecraft position over the visibility windows identified in Point 1 and deriving the associated expected measurements.

   (b) Simulating the measurements by adding a random error to the expected measurements (assume a Gaussian model to generate the random error, with noise provided in Table 4). Discard any measurements (i.e., after applying the noise) that does not fulfill the visibility condition for the considered station.

3. *Solve the navigation problem.* Using the measurements simulated at the previous point:

   (a) Find the least squares (minimum variance) solution to the navigation problem without a priori information using
   - the epoch t_0 as reference epoch;
   - the reference state as the state derived from the TLE set in Table 2 at the reference epoch;
   - the simulated measurements obtained for the KOROU ground station only;
   - pure Keplerian motion to model the spacecraft dynamics.

   (b) Repeat step 3a by using all simulated measurements from both ground stations.

   (c) Repeat step 3b by using J2-perturbed motion to model the spacecraft dynamics.

4. Provide the obtained navigation solutions and elaborate on the results, comparing the different solutions.

5. Select the best combination of dynamical model and ground stations and perform the orbit determination for the other satellite.

Table 2: TLE of Mango.

```
1 36599U 10028B   10224.22752732 -.00000576  00000-0 -16475-3 0  9998
2 36599 098.2803 049.5758 0043871 021.7908 338.5082 14.40871350  8293
```

Table 3: TLE of Tango.

```
1 36827U 10028F   10224.22753605  .00278492  00000-0  82287-1 0  9996
2 36827 098.2797 049.5751 0044602 022.4408 337.8871 14.40890217    55
```

Table 4: Sensor network to track Mango and Tango: list of stations, including their features.

Station name	KOUROU	SVALBARD
Coordinates	LAT = 5.25144° LON = -52.80466° ALT = -14.67 m	LAT = 78.229772° LON = 15.407786° ALT = 458 m
Type	Radar (monostatic)	Radar (monostatic)
Provided measurements	Az, El [deg] Range (one-way) [km]	Az, El [deg] Range (one-way) [km]
Measurements noise (diagonal noise matrix R)	$\sigma_{Az,El}$ = 100 mdeg σ_{range} = 0.01 km	$\sigma_{Az,El}$ = 125 mdeg σ_{range} = 0.01 km
Minimum elevation	10 deg	5 deg

1) Using two-body Keplerian dynamics, Mango's initial mean state $\hat{\mathbf{x}}_{0,M}$ at t_{sep} is propagated first up to t_0, then from from t_0 to t_f over the defined time grid.
At each time instant t, the predicted state is converted into Azimuth, Elevation and range measurements for both KOUROU and SVALBARD stations.

The conversion from ECI state into measurements is performed by the function `antenna_pointing`, which first computes the relative position of the satellite with respect to the station topocentric earth fixed frame $\mathbf{r}_{M-ST}^{TOPO}$, then the associated measurements:

$$\mathbf{r}_{M-ST}^{TOPO} = R_{TOPO/ECI}\mathbf{r}_{M}^{ECI} - \mathbf{r}_{ST}^{TOPO}$$

$$\mathbf{y} = \begin{bmatrix} Az \\ El \\ r \end{bmatrix} = \begin{bmatrix} tan^{-1}\left(\dfrac{\mathbf{r}_{M-ST,y}^{TOPO}}{\mathbf{r}_{M-ST,x}^{TOPO}}\right) \\ sin^{-1}\left(\dfrac{\mathbf{r}_{M-ST,x}^{TOPO}}{r_{M-ST}^{TOPO}}\right) \\ r_{M-ST}^{TOPO} \end{bmatrix} = \mathbf{h}\left(\mathbf{r}_{M-ST}^{TOPO}\right) = \mathbf{h}\left(\mathbf{r}_{M}^{ECI}\right)$$

It ought to be noted that the predicted motion computed through Keplerian dynamics is only used for the allocation of the antennas measurement time windows, computed based on the expected measurements that satisfy the constraint $El > El_{min}$ are recorded.
The number of acquired measurements however can differ from the number of expected ones.

Below the visibility windows in UTC time:

KOUROU

1	`2010 AUG 12 08:46:00.000`	`2010 AUG 12 08:54:00.000`
2	`2010 AUG 12 10:27:00.000`	`2010 AUG 12 10:30:00.000`

Expected Visibility	>11 min
Expected Measurements	13

Table 5: Mango expected visibility windows over KOUROU.

SVALBARD		
1	2010 AUG 12 05:44:00.000	2010 AUG 12 05:54:00.000
2	2010 AUG 12 07:26:00.000	2010 AUG 12 07:34:00.000
3	2010 AUG 12 09:08:00.000	2010 AUG 12 09:14:00.000
4	2010 AUG 12 10:50:00.000	2010 AUG 12 10:55:00.000

Expected Visibility	>29 min
Expected Measurements	33

Table 6: Mango expected visibility windows over SVALBARD.

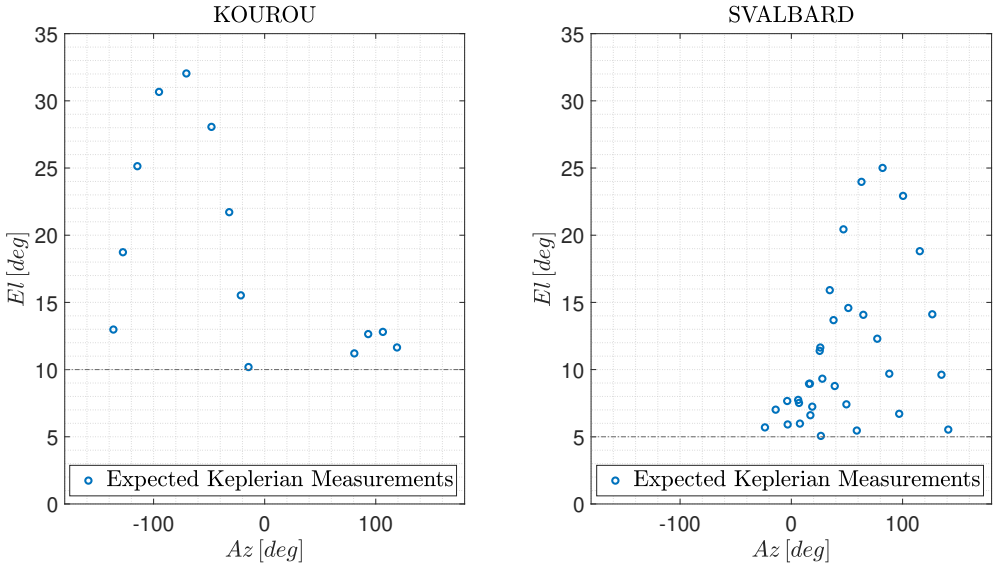

Figure 5: Mango expected apparent motion.

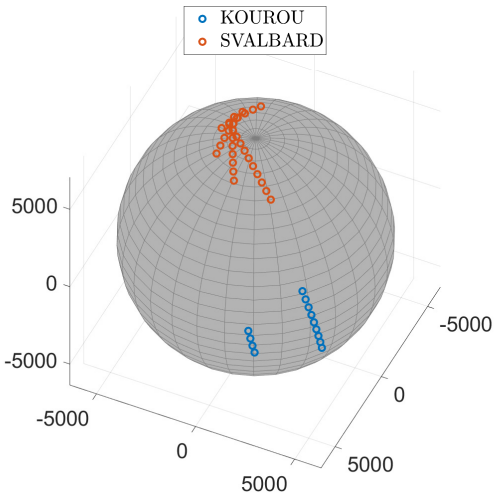

Figure 6: Mango motion representation.

2) The Two-Line Elements set of Mango yields the state of the satellite at reference epoch `2010-08-12 05:27:38.360448 UTC`. It is easy to see that for both KOUROU and SVALBARD the last expected measurement is still within $6h$ of the LTE reference epoch. Therefore, it is possible to assume with good approximation that, over the previously computed visibility windows, SGP4 will be most indicative of the real behaviour of the satellite.

At each instant of the previously defined time grid, in compatibility with the visibility windows, the function `station_measurements` computes the satellite state in TEME reference frame, performs the transformation into ECI, then again exploiting `antenna_pointing` $\mathbf{y}$ is provided. In order to simulate error in the measurement process, random noise is added as realization of a multivariate Gaussian distribution. The measurements $\mathbf{y}$:

$$\mathbf{y} = \mathbf{h}(\mathbf{r}) + \boldsymbol{\epsilon} \quad \text{with} \quad \boldsymbol{\epsilon} \sim G\left(\mathbf{0}, \begin{bmatrix} \sigma_{Az}^2 & 0 & 0 \\ 0 & \sigma_{El}^2 & 0 \\ 0 & 0 & \sigma_r^2 \end{bmatrix}\right)$$

$R = \begin{bmatrix} \sigma_{Az}^2 & 0 & 0 \\ 0 & \sigma_{El}^2 & 0 \\ 0 & 0 & \sigma_r^2 \end{bmatrix}$ is the noise matrix associated to the radar station.

Measurements that do not satisfy the relative station minimum El requirement are filtered out.

Below the true measurements:

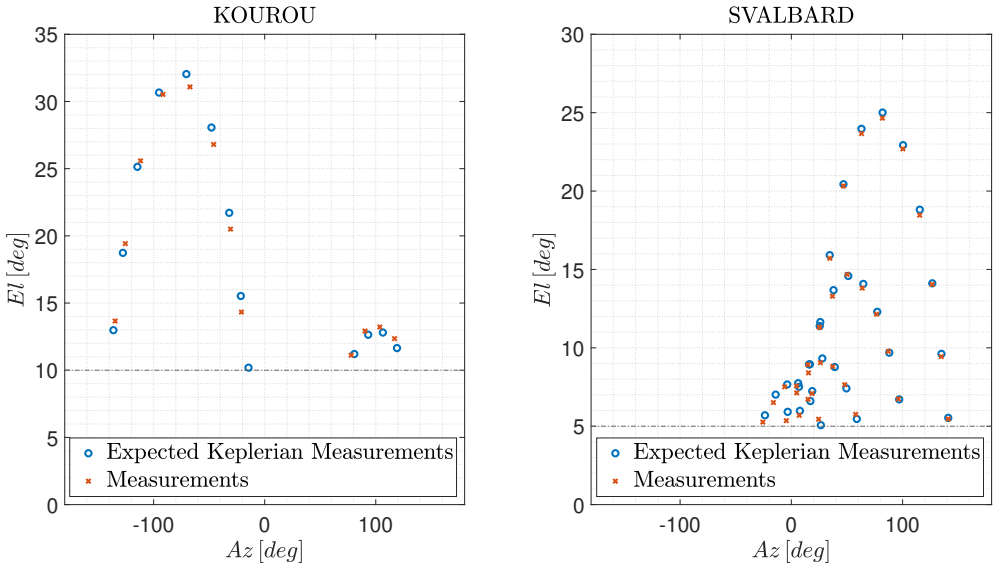

Figure 7: Mango apparent motion.

In the presented graph, it is possible to see that one KOUROU measurements has been filtered out.

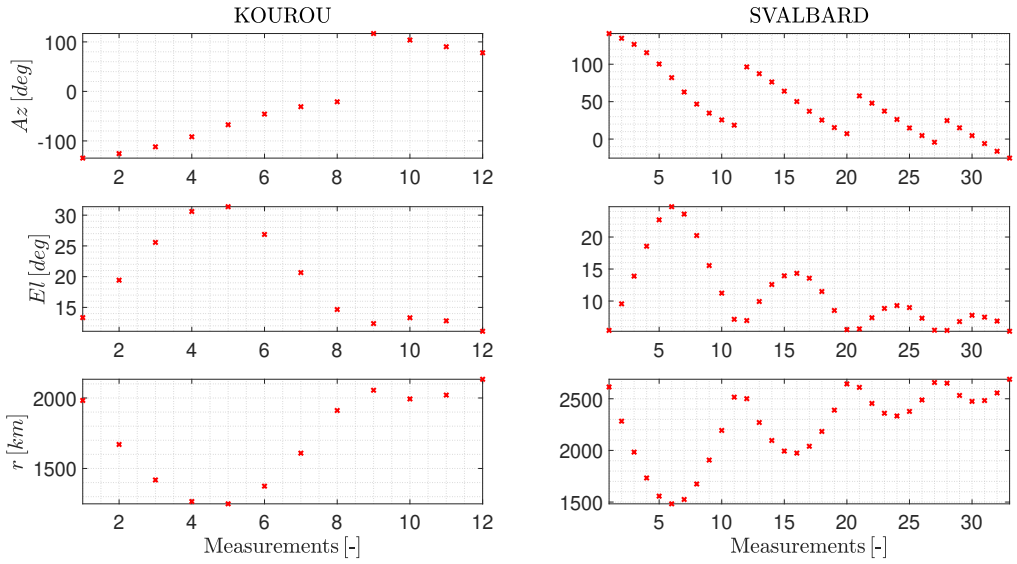

Figure 8: Mango associated measurements.

3) Given the previously computed measurements, a batch filter is implemented in order to estimate the satellite state at t_0. The optimality of the estimate is evaluated in terms of Weighted Least Squares of the residuals.

   Given a batch of measurements $\mathbf{y}_i$ at specified epochs t_i and the station of reference associated to such measurements, the function `cost_fun` propagates an initial state guess $\mathbf{x}_0^g$ starting from t_0 over the measurement epochs t_i according to specified system dynamics. At every time instant t_i the weighted residuals are computed as follows:

$$\Delta\mathbf{y}_i^W = W\left[\mathbf{y}_i - \mathbf{h}\left(\mathbf{x}^g\left(t_i\right)\right)\right]$$

   Where $\mathbf{x}^g\left(t_i\right)$ is the propagated state $\mathbf{x}_0^g$ evaluated at time t_i, and W the weight matrix associated to the station noise matrix R, computed as $W = \sqrt{R^{-1}}$.

   The solution to Weighted Least Squares problem is found employing the MatLab function `lsqnonlin`. It perturbs the initial guess $\mathbf{x}_0^g$ until the solution $\mathbf{x}_0$ that minimizes the weighted sum of the squares of the residuals is found.

4) Mango estimated initial state is computed using the following combinations of stations and model dynamics:

   I. KOUROU measurements, simple Keplerian motion
   II. KOUROU and SVALBARD measurements, simple Keplerian motion
   III. KOUROU and SVALBARD measurements, Keplerian motion with J_2 perturbation

   The J_2 effect is modeled as a perturbative acceleration to be added to that of simple Keplerian motion. The symbol $\odot$ indicates the Hadamard element-wise multiplication:

$$\ddot{\mathbf{r}} = -\mu\frac{\mathbf{r}}{r^3} + \mathbf{a}_{J_2} \qquad \mathbf{r}_{ECEF} = R_{ECEF/ECI}\mathbf{r}$$

$$\mathbf{a}_{J_2} = R_{ECEF/ECI}^{\mathsf{T}}\left[\frac{3}{2}\mu J_2\frac{\mathbf{r}_{ECEF}}{r_{ECEF}^3}\left(\frac{R_E}{r_{ECEF}}\right)^2 \odot \left(5\left(\frac{r_{ECEF,z}}{r_{ECEF}}\right)^2\begin{Bmatrix}1\\1\\1\end{Bmatrix} - \begin{Bmatrix}1\\1\\3\end{Bmatrix}\right)\right]$$

	Estimated state $\mathbf{x}_{0,M}$ $[km, km/s]$
I	[4664.6664, 5248.7677, 1043.5812, 0.0615, −1.5468, 7.3515]
II	[4666.2960, 5248.9428, 1039.6092, 0.0921, −1.5478, 7.3503]
III	[4685.4088, 5238.5805, 1042.5653, 0.0816, −1.5566, 7.3445]

In first approximation, it possible to compare the different solutions in terms of the covariance of the solutions P_{LSQ}. Given N_M measurements and n state components:

$$P_{LSQ} = \frac{\sum_{i=1}^{N_M} \|\Delta \mathbf{y}_i^W\|^2}{N_M - n} [J^\intercal J] \quad \text{with} \quad (J)_{i,j} = \frac{\partial \Delta \mathbf{y}_i^W}{\partial x_j}$$

The standard deviations, expressed in terms of square root of the traces of the position and velocity submatrices, are indicative of the uncertainty associated to the estimated state $\mathbf{x}_{0,M}$:

	$\sigma_r\,[km]$	$\sigma_v\,[km/s]$
I	3.9554×10^{1}	1.4230×10^{-1}
II	5.8526×10^{-1}	7.7092×10^{-4}
III	8.4672×10^{-3}	1.0432×10^{-5}

The true indicators of the estimation however are in fact the residuals $\Delta \mathbf{y}_i$.
Below their absolute value per each measurement, for each computed solution:

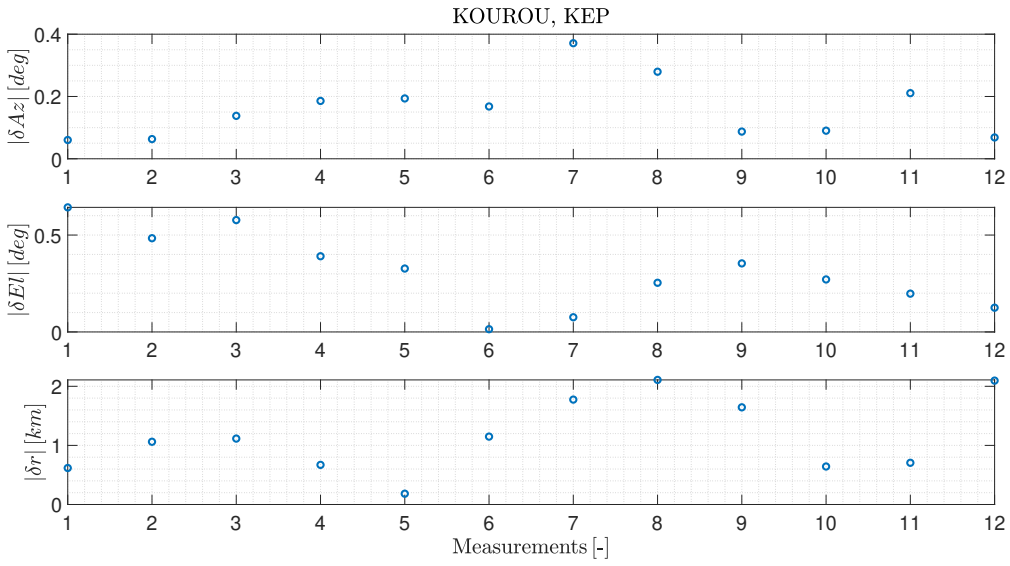

Figure 9: Residuals of KOUROU measurements, simple Keplerian dynamics (I).

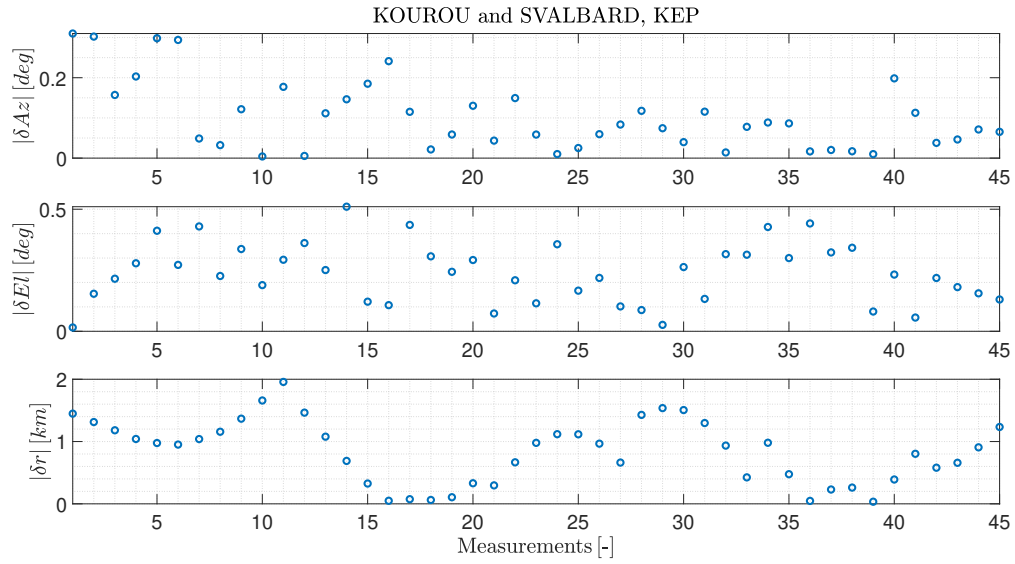

Figure 10: Residuals of KOUROU and SVALBARD measurements, simple Keplerian dynamics (II).

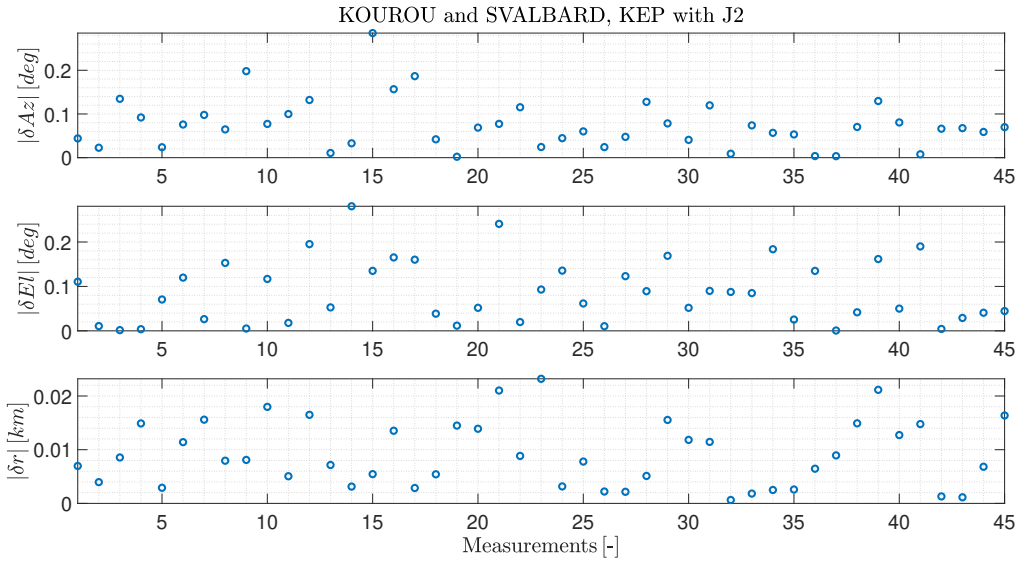

Figure 11: Residuals of KOUROU and SVALBARD measurements, Keplerian dynamics with J_2 perturbation (III).

The mean values associtated to the presented residuals, per method:

	$\lvert\delta Az\rvert$	$\lvert\delta El\rvert$	$\lvert\delta r\rvert$
I	2.4793×10^{-1}	2.5035×10^{-1}	5.9519×10^{-1}
II	1.5120×10^{-1}	2.3266×10^{-1}	8.3487×10^{-1}
III	9.0976×10^{-2}	9.7189×10^{-2}	9.1334×10^{-3}

Table 7: Measurements residuals means.

The performance of a batch filter is directly proportional to the number of acquired measurements, their spread along the orbit and to the ability of the employed dynamical model to capture the real system behaviour.

Between method I and II, which exploit the same dynamical model, there is no direct increase in precision, but rather a slight trade-off of azimuthal precision in favour of range accuracy. Method II employs $N_M^{II} \approx 4N_M^I$ measurements, but at the same time SVALBARD angular measurement precision is slightly worse.
Using two stations however allows better capturing of the orbital shape, therefore increasing range precision, as both equatorial and polar states are observed. Both methods are however limited by the choice of system dynamics: given that both satellites are characterized by LEOs the perturbative J_2 effect is not negligible.
The increased precision of method III is apparent: globally the residuals in terms of δAz and δEl are decreased by a factor of ≈ 2, while the precision in terms of δr is increased by a factor of ≈ 100.

Method III is therefore deemed the most reliable for the given satellite.

5) The visibility windows for Tango are computed in the same fashion as for those of Mango. Given that the two satellites fly in close formation the visibility windows result to be the same of Mango Table 5, Table 10.

Below the acquired measurements:

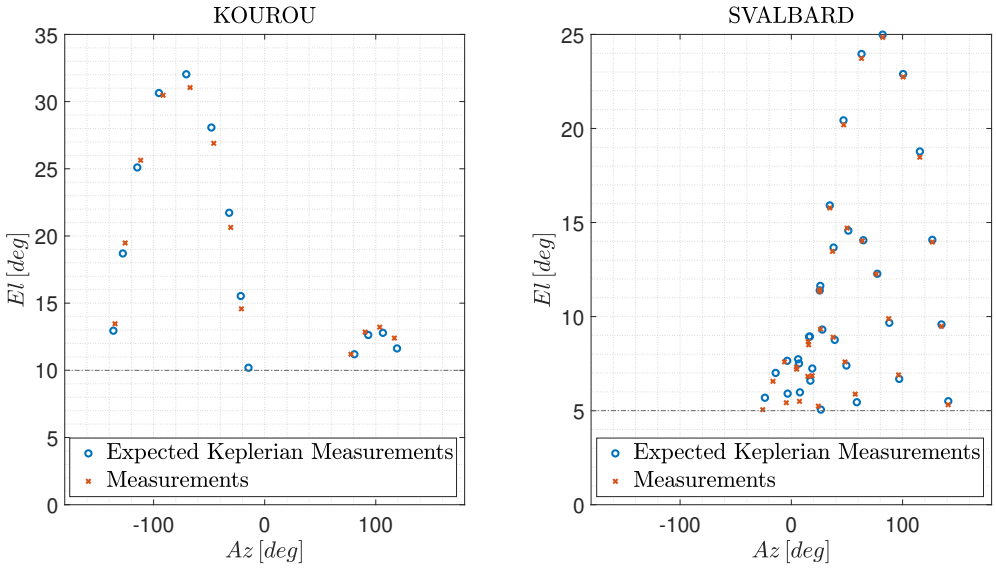

Figure 12: Tango apparent motion.

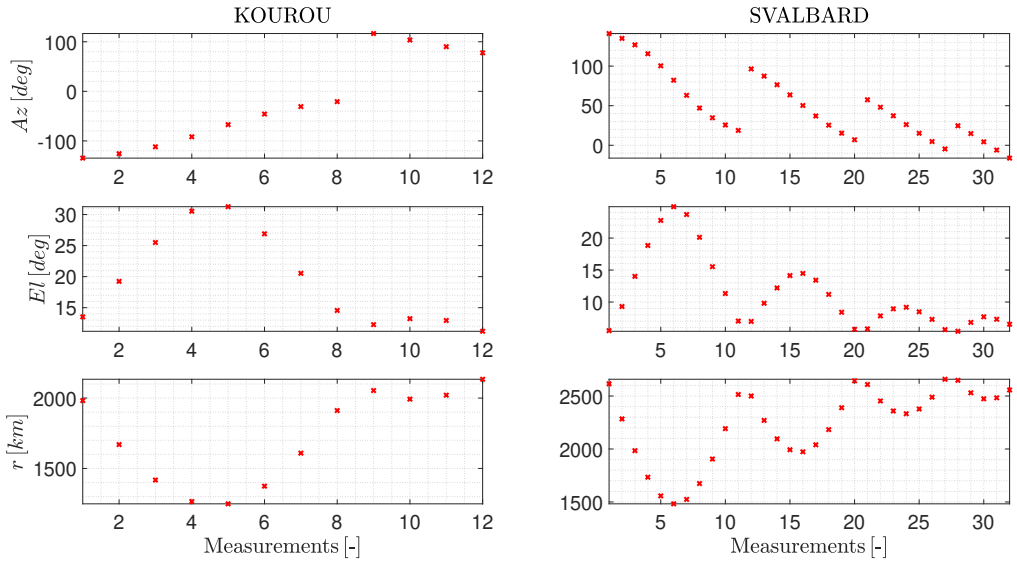

Figure 13: Tango associated measurements.

The state $\mathbf{x}_{0,T}$ estimation is performed using both KOUROU and SVALBARD measurements, given Keplerian dynamics with J_2 perturbation.

	Estimated state $\mathbf{x}_{0,T}$ $[km,\ km/s]$
III	$[4685.0409,\ 5238.8116,\ 1039.2276,\ 0.0835,\ -1.5545,\ 7.3454]$

	$\sigma_r\,[km]$	$\sigma_v\,[km/s]$
III	1.4699×10^{-1}	1.6532×10^{-4}

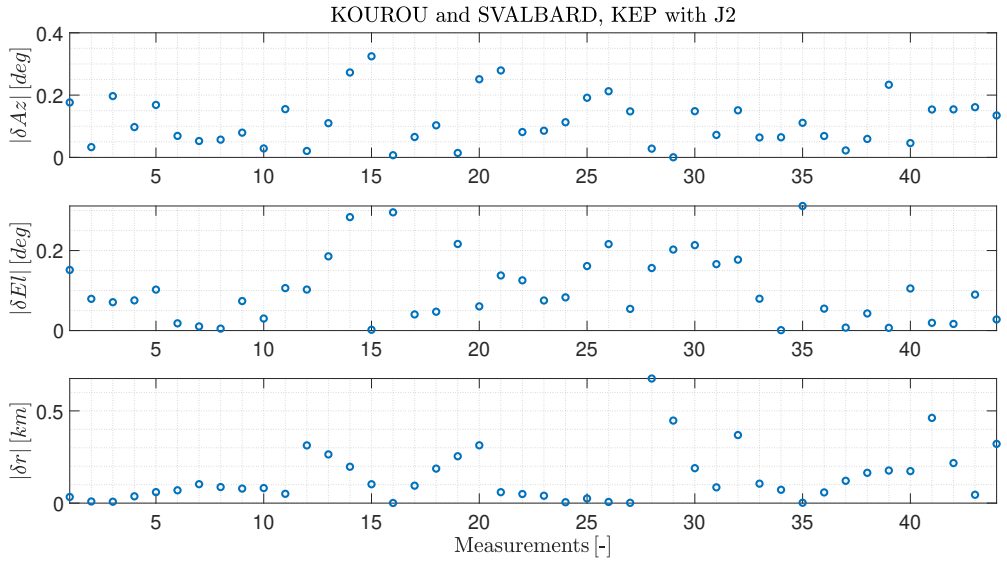

Figure 14: Residuals of KOUROU and SVALBARD measurements, Keplerian dynamics with J_2 perturbation.

It's worth noting that using an equal number of measurements and same dynamical model, method III, the estimation yields a worse result. In fact the residuals associated to the measurements of Tango are higher, especially in terms of range δ_r.
This is attributable to the dynamical model of choice, which results do be effectively descriptive of Mango's motion but not of Tango's.
The two satellites are in fact characterized by a very different B^* drag coefficient. From the respective TLE:

$$B^*_M = -1.6475 \times 10^{-4}\, m^{-1} \quad B^*_T = 8.2287 \times 10^{-2}\, m^{-1}$$

B^* is indicative of the unmodeled perturbative forces acting on a satellite.
To increase the precision of the results associated to Tango, the dynamical model would require further refining.

Exercise 3: Sequential filters

According to the Formation Flying In Orbit Ranging Demonstration experiment (FFIORD), PRISMA's primary objectives include testing and validation of GNC hardware, software, and algorithms for autonomous formation flying, proximity operations, and final approach and recede operations. The cornerstone of FFIORD is a Formation Flying Radio Frequency (FFRF) metrology subsystem designed for future outer space formation flying missions.

FFRF subsystem is in charge of the relative positioning of 2 to 4 satellites flying in formation. Each spacecraft produces relative position, velocity and line-of-sight (LOS) of all its companions.

You have been asked to track Mango to improve the accuracy of the estimate of its absolute state and then, according to the objectives of the PRISMA mission, validate the autonomous formation flying navigation operations by estimating the relative state between Mango and Tango by exploiting the relative measurements acquired by the FFRF subsystem. The Two-Line Elements (TLE) set of Mango and Tango satellites are reported in Tables 2 and 3 (and in WeBeep as 36599.3le, and 36827.3le).

The relative motion between the two satellites can be modelled through the linear, Clohessy-Wiltshire (CW) equations[†]

$$\begin{aligned} \ddot{x} &= 3n^2 x + 2n\dot{y} \\ \ddot{y} &= -2n\dot{x} \\ \ddot{z} &= -n^2 z \end{aligned} \tag{1}$$

where x, y,and z are the relative position components expressed in the LVLH frame, whereas n is the mean motion of Mango, which is assumed to be constant and equal to:

$$n = \sqrt{\frac{GM}{R^3}} \tag{2}$$

where R is the position of Mango at t_0.

The unit vectors of the LVLH reference frame are defined as follows:

$$\hat{\boldsymbol{i}} = \frac{\boldsymbol{r}}{r}, \quad \hat{\boldsymbol{j}} = \hat{\boldsymbol{k}} \times \hat{\boldsymbol{i}}, \quad \hat{\boldsymbol{k}} = \frac{\boldsymbol{h}}{h} = \frac{\boldsymbol{r} \times \boldsymbol{v}}{\|\boldsymbol{r} \times \boldsymbol{v}\|} \tag{3}$$

To perform the requested tasks you should:

1. *Estimate Mango absolute state.* You are asked to develop a sequential filter to narrow down the uncertainty on the knowledge of Mango absolute state vector. To this aim, you shall schedule the observations from the SVALBARD ground station[‡] reported in Table 4, and then proceed with the state estimation procedure by following these steps:

   (a) By using the mean state reported in Table 1 and by assuming Keplerian motion, predict the trajectory of the satellite over a uniform time grid (with a time step of 5 seconds) and compute the first visibility time window from the SVALBARD station in the time interval from t_0 = `2010-08-12T05:30:00.000` (UTC) to t_f = `2010-08-12T06:30:00.000` (UTC).

   (b) Use SGP4 and the provided TLE to simulate the measurements acquired by the SVALBARD station for the Mango satellite only. For doing it, compute the spacecraft position over the visibility window using a time-step of 5 seconds, and derive the associated expected measurements. Finally, simulate the measurements by adding a random error (assume a Gaussian model to generate the random error, with noise provided in Table 4).

[†]Notice that the system is linear, therefore it has an analytic solution of the state transition matrix $\boldsymbol{\Phi}$

[‡]Note that these are the same ones computed in Exercise 2

(c) Using an Unscented Kalman Filter (UKF), provide an estimate of the spacecraft state (in terms of mean and covariance) by sequentially processing the acquired measurements in chronological order. Plot the time evolution of the error estimate together with the 3σ of the estimated covariance for both position and velocity.

2. *Estimate the relative state.* To validate the formation flying operations, you are also asked to develop a sequential filter to narrow down the uncertainty on the knowledge of the relative state vector. To this aim, you can exploit the relative azimuth, elevation, and range measurements obtained by the FFRF subsystem, whose features are reported in Table 8, and then proceed with the state estimation procedure by following these steps:

   (a) Use SGP4 and the provided TLEs to propagate the states of both satellites at epoch t_0 in order to compute the relative state in LVLH frame at that specific epoch.

   (b) Use the relative state as initial condition to integrate the CW equations over the time grid defined in Point 1a. Finally, simulate the relative measurements acquired by the Mango satellite through its FFRF subsystem by adding a random error to the expected measurements. Assume a Gaussian model to generate the random error, with noise provided in Table 8.

   (c) Consider a time interval of 20 minutes starting from the first epoch after the visibility window (always with a time step of 5 seconds). Use an UKF to provide an estimate of the spacecraft relative state in the LVLH reference frame (in terms of mean and covariance) by sequentially processing the measurements acquired during those time instants in chronological order. Plot the time evolution of the error estimate together with the 3σ of the estimated covariance for both relative position and velocity.

3. *Reconstruct Tango absolute covariance.* Starting from the knowledge of the estimated covariance of the absolute state of Mango, computed in Point 1, and the estimated covariance of the relative state in the LVLH frame, you are asked to provide an estimate of the covariance of the absolute state of Tango. You can perform this operation as follows:

   (a) Pick the estimated covariance of the absolute state of Mango at the last epoch of the visibility window, and propagate it within the time grid defined in Point 2c.

   (b) Rotate the estimated covariance of the relative state from the LVLH reference frame to the ECI one within the same time grid.

   (c) Sum the two to obtain an estimate of the covariance of the absolute state of Tango. Plot the time evolution of the 3σ for both position and velocity and elaborate on the results.

Table 8: Parameters of FFRF.

Parameter	Value
Measurements noise (diagonal noise matrix R)	$\sigma_{Az,El} = 1$ deg $\sigma_{range} = 1$ cm

1) As per the previous exercise, the antenna measurement window allocation is based on Keplerian prediction. The computed visibility window slightly differs from that of the first row of Table 10, as the measuring period is lower.

   The updated visibility window:

SVALBARD	
2010 AUG 12 05:43:55.000	2010 AUG 12 05:54:35.000

Expected Visibility	>10.67 min
Expected Measurements	129

Table 9: Mango expected visibility windows over SVALBARD.

Having demonstrated it being more precise for the prediction of the satellites' motion, Keplerian dynamics henceforward incorporate J_2 perturbation.

The measurements acquired by the station are simulated in the same fashion as per section 2. Below the satellite apparent motion with respect to the station and the acquired measurements:

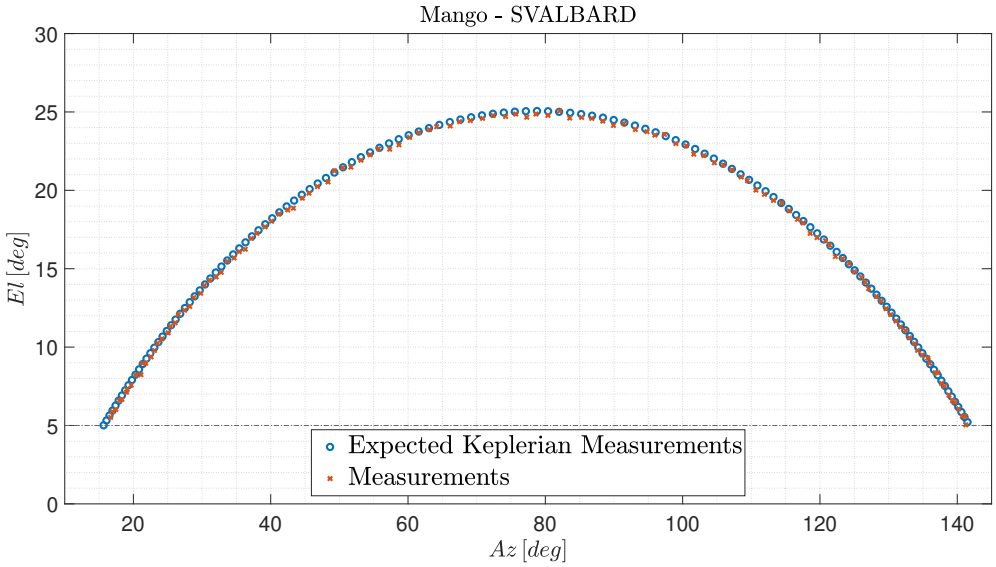

Figure 15: Mango apparent motion.

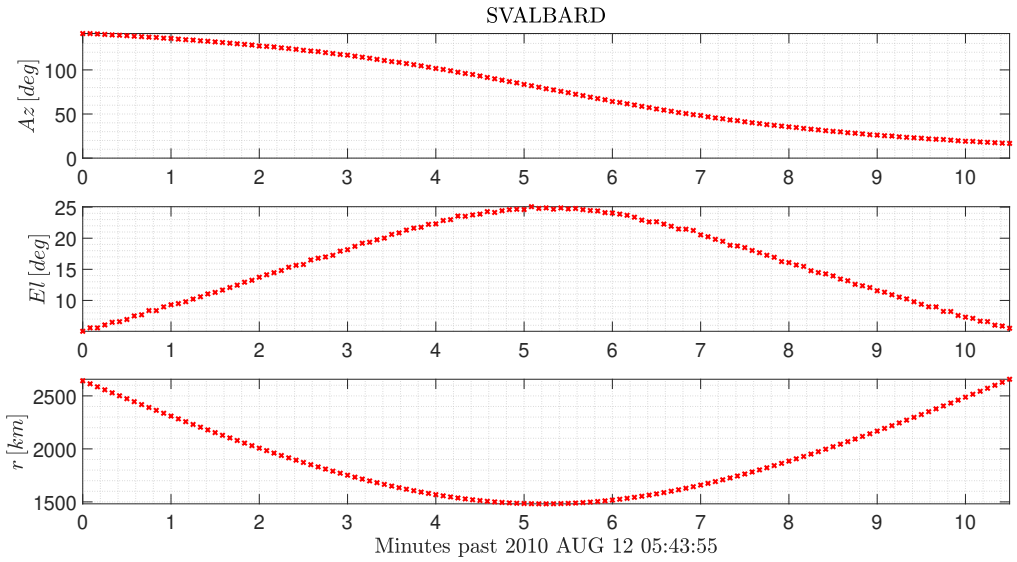

Figure 16: SVALBARD measurements.

An Unscented Kalman Filter is implemented in order to sequentially filter the state estimate given the acquired measurements.
Starting from initial condition $\hat{\mathbf{x}}_{s,1} = \hat{\mathbf{x}}_{0,sat1}$ and $P_s = P_0 \times 10^4$ at t_{sep}, at each measurement epoch t_j an estimate of the propagated state $\hat{\mathbf{x}}_1(t_j)$ and covariance $P(t_i)$ are computed by means of prediction and correction.
The prediction is performed via Unscented Transform as per section 1. The tuning parameters α, β and k are unchanged. The prediction yields a priori estimates $\hat{\mathbf{x}}^-(t_i)$ and $P^-(t_i)$, corrected to $\hat{\mathbf{x}}(t_i)$ and $\widetilde{P}(t_i)$ by exploitation of the innovation introduced by the measurement $\mathbf{y}_i$ at t_i.
At each iteration a symmetry correction is also applied to $\widetilde{P}(t_i)$ to filter out numerical error:

$$P(t_i) = \frac{\widetilde{P}(t_i) + \widetilde{P}^{\intercal}(t_i)}{2}$$

Below the results associated to the filtering process. The state is presented in terms of absolute position $\delta\mathbf{r}$ and velocity $\delta\mathbf{v}$ displacement computed with respect to the SGP4 computed state, and the $3\sigma_{\mathbf{r}}$, $3\sigma_{\mathbf{v}}$ boundaries as $3\sqrt{tr\left(P_{\mathbf{rr}}(t_i)\right)}$ and $3\sqrt{tr\left(P_{\mathbf{vv}}(t_i)\right)}$ respectively. Henceforth, all 3σ computations will be performed in this fashion.

The results computed at the last measurement:

$\lvert\delta\mathbf{r}\rvert = 2.7385 \times 10^{-2}\, km$	$3\sigma_{\mathbf{r}} = 3.2779 \times 10^{-1}\, km$
$\lvert\delta\mathbf{v}\rvert = 9.4144 \times 10^{-5}\, km/s$	$3\sigma_{\mathbf{v}} = 4.8794 \times 10^{-4}\, km/s$

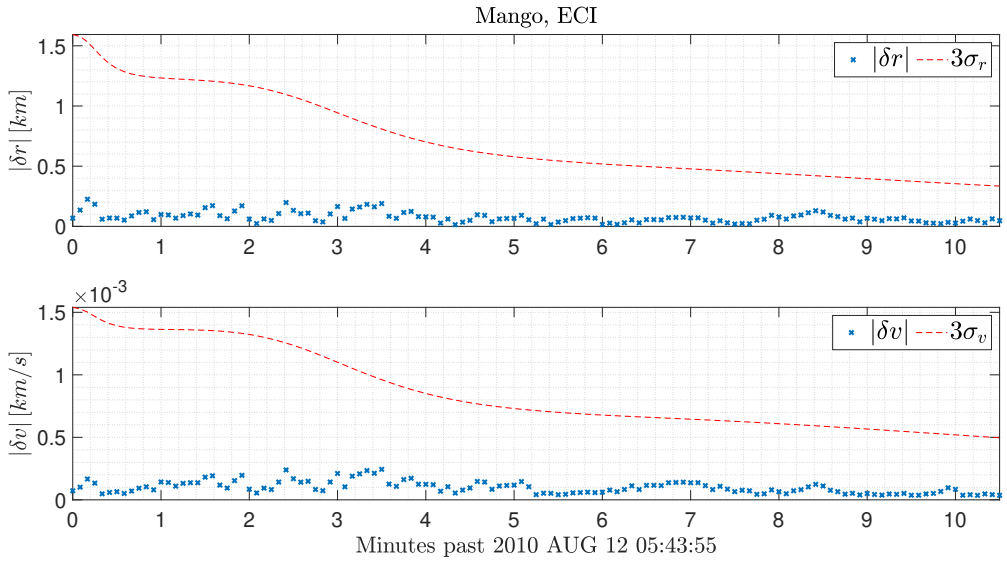

Figure 17: Estimate displacement with respect to SGP4 reference trajectory.

2) In order to perform the rotation of an arbitrary state $\mathbf{x}$ from ECI to the corresponding LVLH frame it is necessary to compute the state rotation matrix $\mathcal{R}_{LVLH/ECI}$, function of $\mathbf{x}$:

$$\mathcal{R}_{LVLH/ECI}(\mathbf{x}) = \begin{bmatrix} R_{LVLH/ECI}(\mathbf{x}) & 0_{3\times 3} \\ \dot{R}_{LVLH/ECI}(\mathbf{x}) & R_{LVLH/ECI}(\mathbf{x}) \end{bmatrix}$$

Its submatrices $R_{LVLH/ECI}$ and $\dot{R}_{LVLH/ECI}$ are function of the LVLH unit vectors defined in Eq. (3) and constructed as:

$$R_{LVLH/ECI}(\mathbf{x}) = \begin{bmatrix} \hat{\mathbf{i}}^\intercal \\ \hat{\mathbf{j}}^\intercal \\ \hat{\mathbf{k}}^\intercal \end{bmatrix} \quad \dot{R}_{LVLH/ECI}(\mathbf{x}) = \begin{bmatrix} \dot{\hat{\mathbf{i}}}^\intercal \\ \dot{\hat{\mathbf{j}}}^\intercal \\ \dot{\hat{\mathbf{k}}}^\intercal \end{bmatrix}$$

The derivatives of the unit vectors depend on the dynamical model of choice. In the case of Keplerian dynamics with J_2 perturbation:

$$\begin{cases} \dot{\hat{\mathbf{i}}} = \dfrac{1}{r}\left[\mathbf{v} - \left(\hat{\mathbf{i}}\cdot\mathbf{v}\right)\hat{\mathbf{i}}\right] \\ \dot{\hat{\mathbf{k}}} = \dfrac{1}{\|\mathbf{r}\wedge\mathbf{v}\|}\left\{\mathbf{r}\wedge\mathbf{a}_{J_2} - \left[\hat{\mathbf{k}}\cdot(\mathbf{r}\wedge\mathbf{a}_{J_2})\right]\hat{\mathbf{k}}\right\} \\ \dot{\hat{\mathbf{j}}} = \dot{\hat{\mathbf{k}}}\wedge\hat{\mathbf{i}} + \hat{\mathbf{k}}\wedge\dot{\hat{\mathbf{i}}} \end{cases}$$

It ought to be noted that if no disturbances were added $\dot{\hat{\mathbf{k}}} = 0$.

The relative state between the two satellites is computed in ECI reference frame exploiting SGP4 at t_0 as:

$$\mathbf{x}_r^{ECI}(t_0) = \mathbf{x}_2(t_0) - \mathbf{x}_1(t_0)$$

It is to be observed with respect to Mango's LVLH reference frame, therefore the following rotation is applied:

$$\mathbf{x}_r(t_0) = \mathcal{R}_{LVLH/ECI}(\mathbf{x}_1(t_0))\,\mathbf{x}_r^{ECI}(t_0)$$

The relative state is then propagated in time according to the Clohessy-Wiltshire equations, to describe the motion of Tango with respect to Mango in Mango's LVLH frame:

$$\dot{\mathbf{x}} = \begin{bmatrix} 0 & 0 & 0 & 1 & 0 & 0 \\ 0 & 0 & 0 & 0 & 1 & 0 \\ 0 & 0 & 0 & 0 & 0 & 1 \\ 3n_M^2 & 0 & 0 & 0 & 2n_M & 0 \\ 0 & 0 & 0 & -2n_M & 0 & 0 \\ 0 & 0 & -n_M^2 & 0 & 0 & 0 \end{bmatrix} \mathbf{x} = A_{CW}\mathbf{x}$$

The CW equations are noticeably linear, therefore there exists an algebraic close solution in the form of:

$$\mathbf{x}(t) = e^{A_{CW}(t-t_0)}\mathbf{x}(t_0)$$

Noting that a $\mathbf{x}(t_0) = \mathbf{0}$ yields $\mathbf{x}(t) = \mathbf{0}\,\forall t$, it is possible to rewrite the analytical solution in terms of linearized displacements:

$$\mathbf{x}(t) = \mathbf{x}(t) - \mathbf{0} = \mathbf{\Phi}(t)(\mathbf{x}(t_0) - \mathbf{0}) = \mathbf{\Phi}(t)\mathbf{x}(t_0)$$

The STM $\mathbf{\Phi}(t)$ has closed form solution, function of the mean motion of Mango n_M and time $\Delta t = t - t_0$:

$$\mathbf{\Phi}(t) = \begin{bmatrix} \mathbf{\Phi}(t)_{\mathbf{rr}} & \mathbf{\Phi}(t)_{\mathbf{rv}} \\ \mathbf{\Phi}(t)_{\mathbf{vr}} & \mathbf{\Phi}(t)_{\mathbf{vv}} \end{bmatrix}$$

$$\mathbf{\Phi}(t)_{\mathbf{rr}} = \begin{bmatrix} 4 - 3cos(n_M\Delta t) & 0 & 0 \\ 6(sin(n_M\Delta t) - n_M\Delta t) & 1 & 0 \\ 0 & 0 & cos(n_M\Delta t) \end{bmatrix}$$

$$\mathbf{\Phi}(t)_{\mathbf{rv}} = \begin{bmatrix} sin(n_M\Delta t)/n_M & 2(1 - cos(n_M\Delta t))/n_M & 0 \\ 2(cos(n_M\Delta t) - 1)/n_M & (4sin(n_M\Delta t) - 3n_M\Delta t)/n_M & 0 \\ 0 & 0 & sin(n_M\Delta t)/n_M \end{bmatrix}$$

$$\mathbf{\Phi}(t)_{\mathbf{vr}} = \begin{bmatrix} 3n_M sin(n_M\Delta t) & 0 & 0 \\ 6n_M(cos(n_M\Delta t) - 1) & 0 & 0 \\ 0 & 0 & -n_M sin(n_M\Delta t) \end{bmatrix}$$

$$\mathbf{\Phi}(t)_{\mathbf{vv}} = \begin{bmatrix} cos(n_M\Delta t) & 2sin(n_M\Delta t) & 0 \\ -2sin(n_M\Delta t) & 4cos(n_M\Delta t) - 3 & 0 \\ 0 & 0 & cos(n_M\Delta t) \end{bmatrix}$$

This form is strongly preferable for the purpose of the mission over both the analytical exponential solution and numerical ODE propagation. In fact, it allows Mango to estimate the relative position of Tango at any instant t in one single function evaluation. It is therefore a numerically light method, befit for on-board computation in the perspective of autonomous GNC.
It is therefore employed for both the UKF and measurement simulations. The measurements are simulated starting from initial conditions $\mathbf{x}_r(t_0)$ at given t_0, and recorded over the following time window:

FFRF	
2010 AUG 12 05:54:40.000	2010 AUG 12 06:14:40.000

Table 10: FFRF acquisition window.

The FFRF system collects a total of 241 measurements starting from the first epoch after the expected closure of SVALBARD visibility window.

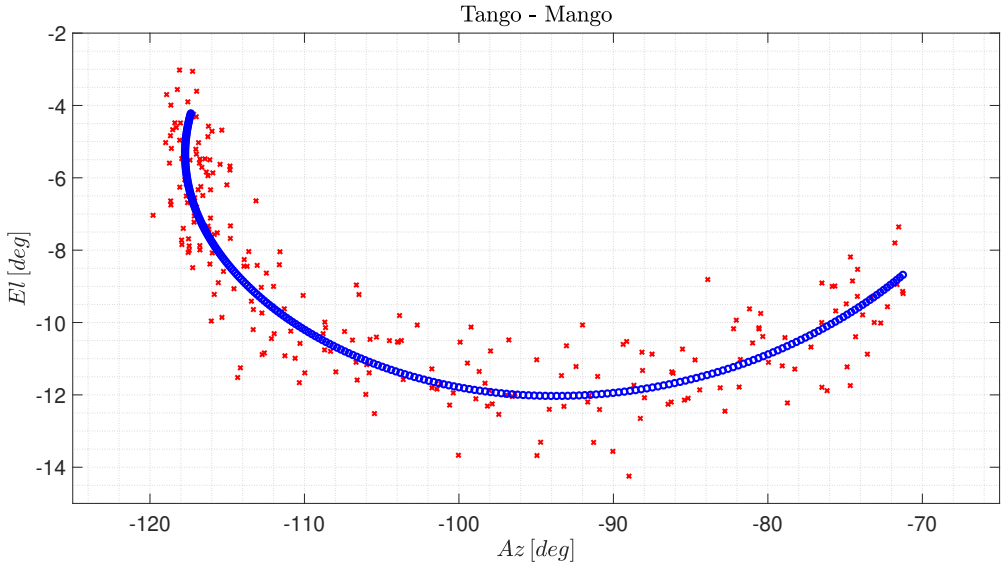

Figure 18: Tango apparent motion with respect to Mango.

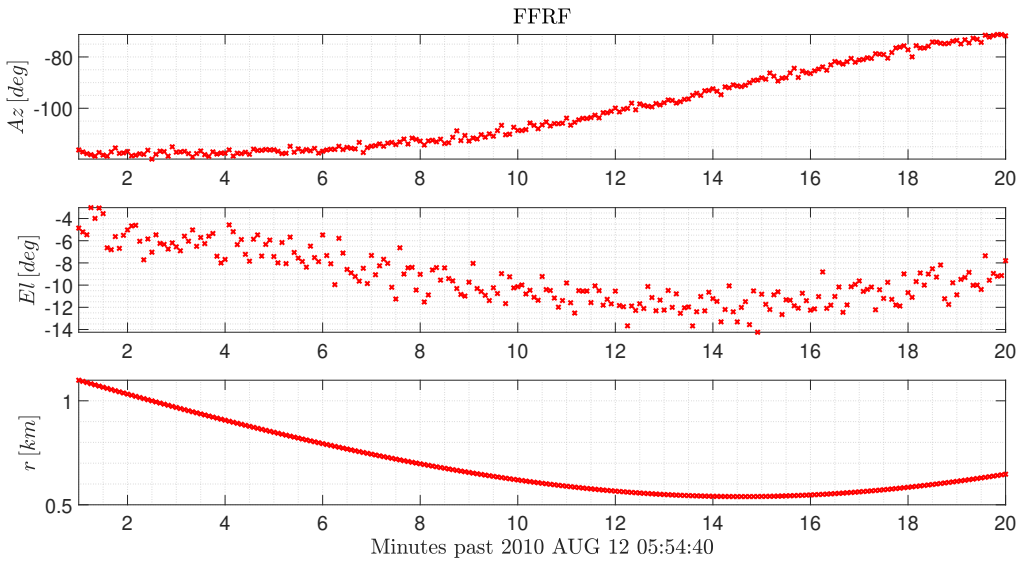

Figure 19: FFRF measurements.

A new UKF is implemented to filter the FFRF acquired measurements, and estimate the relative state of Tango with respect to Mango. It is structurally equivalent to the aforementioned one, but differs in associated dynamic model as the propagation is performed using CW equations.
It is initialized given the states and covariance at t_{sep}:

$$\begin{aligned} \mathbf{x}_r\left(t_{sep}\right) &= \mathcal{R}_{LVLH/ECI}\left(\hat{\mathbf{x}}_{0,1}\left(t_{sep}\right)\right)\left(\hat{\mathbf{x}}_{0,2}-\hat{\mathbf{x}}_{0,1}\right) \\ P_r\left(t_{sep}\right) &= 2\mathcal{R}_{LVLH/ECI}\left(\hat{\mathbf{x}}_{0,1}\left(t_{sep}\right)\right) P_0 \mathcal{R}^{\intercal}_{LVLH/ECI}\left(\hat{\mathbf{x}}_{0,1}\left(t_{sep}\right)\right) \end{aligned}$$

A multiplicative factor of 2 appears in the computation of $P_r\left(t_{sep}\right)$ as result of the combination of the individual uncertainties.

Once again, the results are presented in terms of displacements $\delta\mathbf{r}$, $\delta\mathbf{v}$ and $3\sigma_{\mathbf{r}}$, $3\sigma_{\mathbf{r}}$. The displacements are computed with respect to the reference trajectory defined by the CW propagated initial state $\mathbf{x}_r(t_0)$.

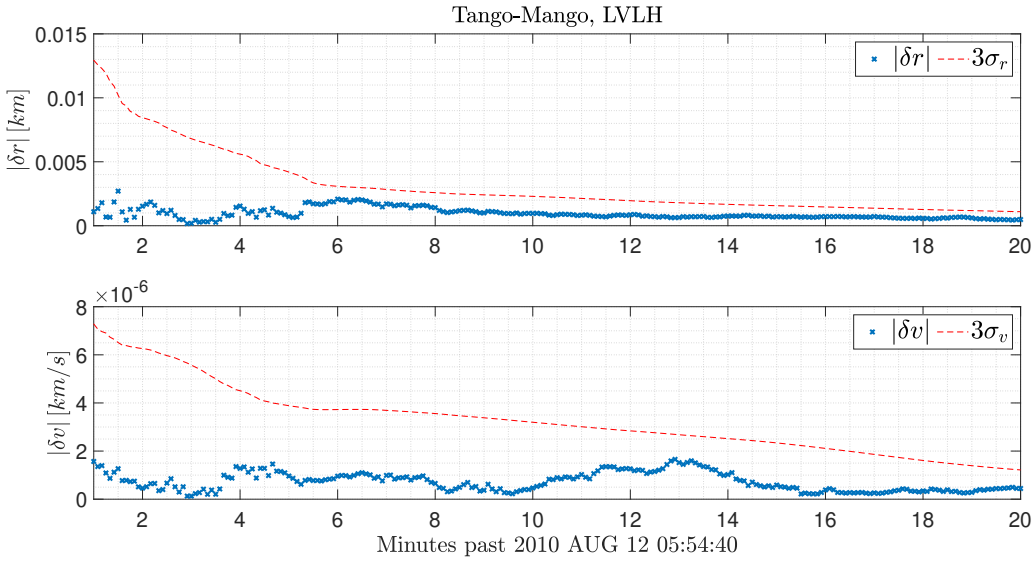

Figure 20: Estimate displacement with respect to CW reference trajectory.

$\lvert\delta\mathbf{r}\rvert = 9.3719 \times 10^{-5}\, km$	$3\sigma_{\mathbf{r}} = 1.1228 \times 10^{-3}\, km$
$\lvert\delta\mathbf{v}\rvert = 5.6245 \times 10^{-7}\, km/s$	$3\sigma_{\mathbf{v}} = 1.1750 \times 10^{-6}\, km/s$

It's worth pointing out that the FFRF system is characterized by high precision in terms of distance measurements, however the noise associated to the angular measurements is relatively high, worse than the one associated to the ground stations. The UKF is however capable of filtering out angular mismeasurements.

3) Starting from the last available UKF absolute estimates of Mango, both state $\hat{\mathbf{x}}_1^{UT}(t)$ and covariance $P_1^{UT}(t)$ are propagated through UT across the FFRF acquisition window time grid.

The relative state and covariance filtered in the previous point are transformed from Mango LVLH frame into ECI. At each FFRF measurement epoch t_i, the transformation is performed as follows:

$$\begin{aligned}
\mathbf{x}_r^{ECI}(t_i) &= \mathcal{R}^{-1}_{LVLH/ECI}\left(\hat{\mathbf{x}}_1^{UT}(t_i)\right)\mathbf{x}_r(t_i) \\
P_r^{ECI}(t_i) &= \mathcal{R}^{-1}_{LVLH/ECI}\left(\hat{\mathbf{x}}_1^{UT}(t_i)\right) P_r(t_i) \left[\mathcal{R}^{\intercal}_{LVLH/ECI}\left(\hat{\mathbf{x}}_1^{UT}(t_i)\right)\right]^{-1} \\
\mathcal{R}^{-1}_{LVLH/ECI}(\mathbf{x}) &= \begin{bmatrix} R^{\intercal}_{LVLH/ECI}(\mathbf{x}) & 0_{3\times 3} \\ \dot{R}^{\intercal}_{LVLH/ECI}(\mathbf{x}) & R^{\intercal}_{LVLH/ECI}(\mathbf{x}) \end{bmatrix}
\end{aligned}$$

Tango's $3\sigma_{\mathbf{r},T}$, $3\sigma_{\mathbf{v},T}$ are extracted from the its absolute covariance, computed as the sum of Mango absolute covariance $P_1^{UT}(t_i)$ and the relative one $P_r^{ECI}(t_i)$.

Below the components associated to the absolute and relative covariances P_1^{UT} and P_r respectively:

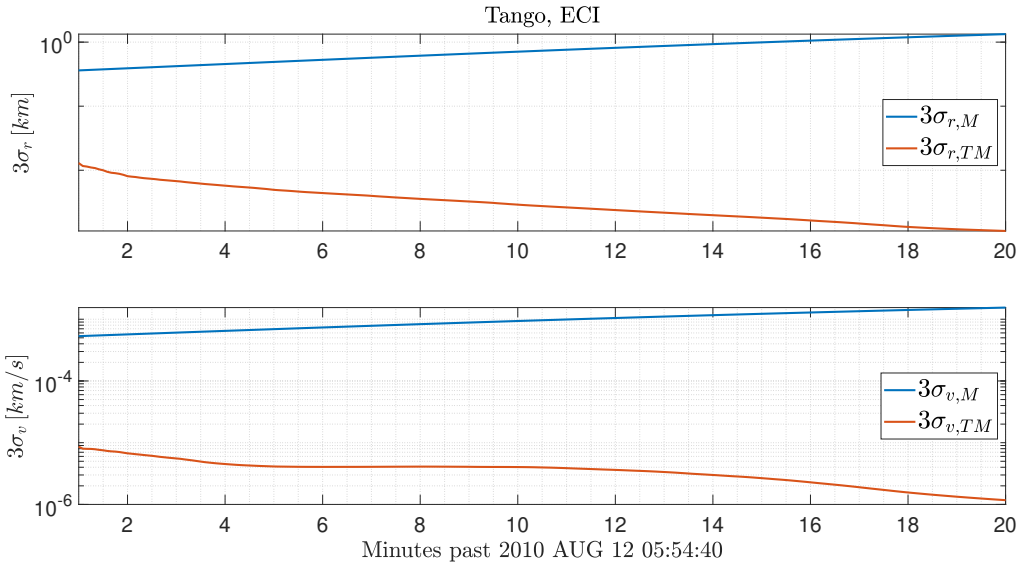

Figure 21: Absolute Mango covariance estimates $3\sigma_M$ and relative covariance estimates $3\sigma_{TM}$ in ECI frame.

It ought to be noted the plot is semi-logarithmic with respect to the y axis.

The converging behaviour associated to the FFRF UKF is completely dominated by the growing uncertainty associated to the UT propagated Mango covariance.

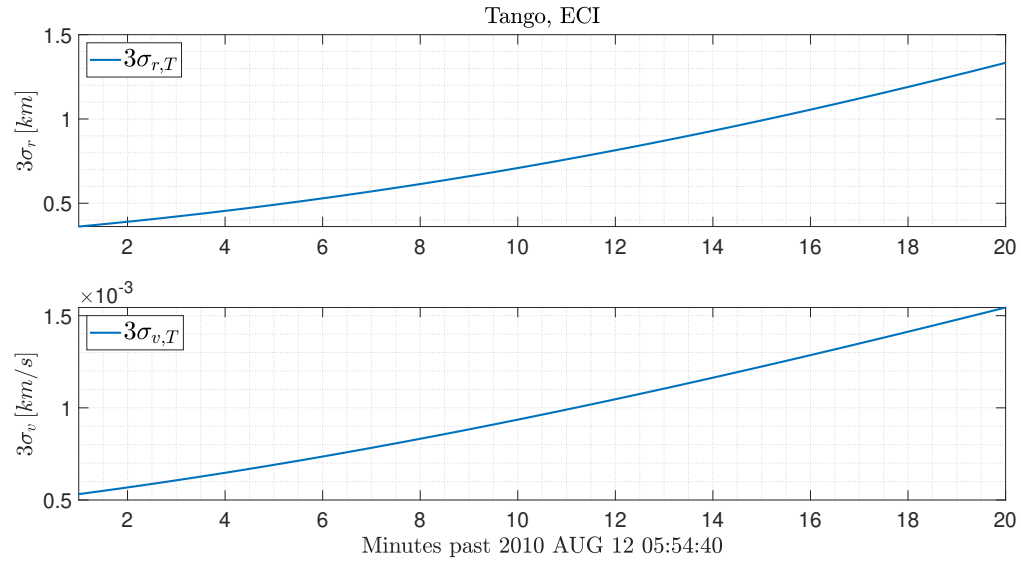

Figure 22: Absolute Tango covariance estimates $3\sigma_T$.